

## Synthetic Aperture Cardiac Imaging with Reduced Number of Acquisition Channels. A Feasibility Study

Yuriy TASINKEVYCH, Marcin LEWANDOWSKI, Ziemowit KLIMONDA, Mateusz WALCZAK

*Institute of Fundamental Technological Research*

*Polish Academy of Sciences*

Pawińskiego 5B, 02-106 Warsaw, Poland; e-mail: yurijtas@ippt.pan.pl

(received December 4, 2017; accepted June 8, 2018)

Commercially available cardiac scanners use 64–128 elements phased-array (PA) probes and classical delay-and-sum beamforming to reconstruct a sector B-mode image. For portable and hand-held scanners, which are the fastest growing market, channel count reduction can greatly decrease the total power and cost of devices. The introduction of ultra-fast imaging methods based on plane waves and diverging waves provides new insight into heart's moving structures and enables the implementation of new myocardial assessment and advanced flow estimation methods, thanks to much higher frame rates. The goal of this study was to show the feasibility of reducing the channel count in the diverging wave synthetic aperture image reconstruction method for phased-arrays. The application of ultra-fast 32-channel sub-aperture imaging combined with spatial compounding allowed the frame rate of approximately 400 fps for 120 mm visualization to be achieved with image quality obtained on par with the classical 64-channel beamformer. Specifically, it was shown that the proposed method resulted in image quality metrics (lateral resolution, contrast and contrast-to-noise ratio), for a visualization depth not exceeding 50 mm, that were comparable with the classical PA beamforming. For larger visualization depths (80–100 mm) a slight degradation of the above parameters was observed. In conclusion, diverging wave phased-array imaging with reduced number of channels is a promising technology for low-cost, energy efficient hand-held cardiac scanners.

**Keywords:** phased-array; ultrasound imaging; diverging wave; synthetic transmit aperture.

### 1. Introduction

Compact portable ultrasound scanners, both general-purpose and specialized, are a fast growing market. The broad range of applications and the wide acceptance of ultrasound diagnostic services and procedures performed under ultrasound imaging (such as biopsy) have created a demand for a new type of apparatus: smaller, more accessible, and designed for a wider population of users, including intermediate health care professionals (SULZBACH-HOKE, SCHANNE, 1999). Among them the portable cardiac scanners may be mentioned which are especially useful in cardiology applications (SERAPHIM *et al.*, 2016), where the speed of diagnosing urgent cases is of primary importance.

A typical heart visualization includes sector 2D B-mode imaging at a speed of 50 fps and 1D M-mode for the imaging of fast moving structures (e.g. valves) at a speed of 1000 lines/s (MOORE *et al.*, 2015). A comprehensive overview of classical cardiac applications is given in (CIKES *et al.*, 2014). Phased-array probes with

transmit beam steering and receive beamforming are now commonly used in cardiac scanners (PAPADACCI *et al.*, 2014). All the elements of the probe are active on each transmit/receive event, thus the system must support the same number of parallel electronic channels. The total number of channels is a very important factor especially for compact/portable systems, because it determines the hardware cost and power consumption (as well as thermal budget). Many low-end portable devices are equipped with only 32 electronic channels, so are limited to linear and convex probes only.

The main objective of this work was to perform a feasibility study of cardiac imaging with reduced channel count acquisition. To this end, a method based on parallel receive beamforming with synthetic transmit aperture diverging wave imaging (HASEGAWA, KANAI, 2011; TONG *et al.*, 2012) has been developed to achieve high-frame-rate (over 400 Hz) echocardiography. To accommodate a low-cost hand-held system requirements, a reduced number of 32 electronic channels was explored in this study to simulate a stan-

dard classical 64 beamforming architecture (or simply beamformer). It should be emphasized that in contrast to the earlier reported methods e.g. the work of PAPADACCI *et al.* (2014) where the authors used a 21-elements sub-aperture on the transmit side and full 64-elements aperture (i.e. 64 electronic channels) on receive side the method proposed in this study uses 32 elemental transducers both in transmit and receive modes which were connected to 32 electronic channels in the corresponding way to accommodate the low-cost system requirements. Moreover, in the cited work (PAPADACCI *et al.*, 2014) the conventional dynamic-focusing beamforming with full aperture was performed in reception for all acquisitions, while in the method discussed in this paper the STA technique was used to reconstruct the final image. An increase in frame rate was achieved through reduction of the number of transmit events. Specifically, the 32-element transmit sub-aperture was laterally translated by a distance of 8-elements between subsequent pulse emissions. In addition, for each sub-aperture position, three beam-steered waves were compounded. In our opinion, the implementation of the presented ultra-fast method would be a key enabler for the development of new portable, compact, lightweight and battery powered USG scanners.

The remainder of the paper is structured as follows: Sec. 2 introduces the theoretical background for synthetic transmit aperture (STA) (TASINKEVYCH *et al.*, 2012b) and diverging wave imaging (DWI) (BAE, JEONG, 2000) methods; Sec. 3 presents the methods, the image quality metrics, and the experimental setup; the experimental results are discussed in Sec. 4, and Sec. 5 concludes the paper.

## 2. Theoretical Background

In the synthetic transmit aperture (STA) imaging approach a transmit sub-aperture comprised of several elements is usually used (TASINKEVYCH *et al.*, 2013) to emit an unfocused wavefront, which interrogates the region of interest in the medium as illustrated in Fig. 1.

The backscattered waves are received by each element independently and the resulting RF echo signals are digitized and stored in memory for further processing. For an  $N$ -element array, a transmit sub-aperture comprised of  $N_t$  elements and  $N_{sh}$ -element translation of the transmit sub-aperture between subsequent emissions, there are  $M = \lceil (N - N_t)/N_{sh} \rceil$  emissions in each data acquisition cycle altogether, where  $\lceil \cdot \rceil$  denotes the integer ceiling of its argument. Then, a coherent summation (delay-and-sum beamforming) of all received RF echoes with dynamic transmit and receive focusing at each imaging point is performed. For an  $N$ -element transducer array at each point in the image the final focused signal can be expressed as follows:

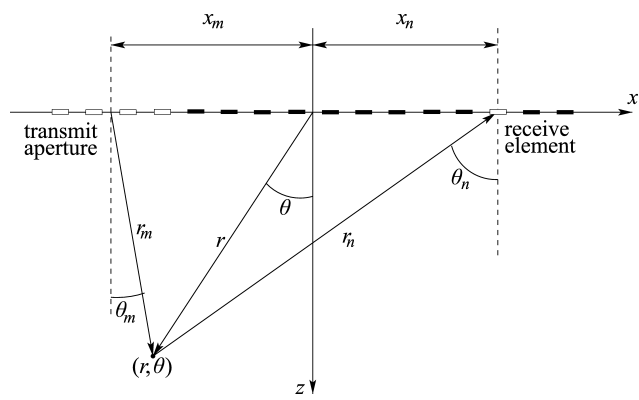


Fig. 1. Spatial diagram illustrating the STA beamforming. The round trip delay is determined by the geometric distance between the imaging point and the transmit sub-aperture and receive element centers.

$$A_{\text{STA}} = \sum_{m=0}^{M-1} \sum_{n=0}^{N-1} s_{m,n}(t - \tau_{m,n}), \quad (1)$$

where  $s_{m,n}(t)$  denotes the RF echo signal recorded by the  $n$ -th receive element and corresponding with the interrogation pulse emitted by the  $m$ -th transmit sub-aperture. The round-trip delay  $\tau_{m,n}$  is determined by the geometric distance from the imaging point to the transmit sub-aperture and then to the receive element, thus is given by the expression:

$$\tau_{m,n} = \tau_m + \tau_n, \quad (2)$$

where the corresponding transmit ( $\tau_m$ ) and receive ( $\tau_n$ ) delays, relative to the focal point  $(r, \theta)$ , are:

$$\tau_i = \frac{r - \sqrt{r^2 + x_i^2 - 2rx_i \cos \theta}}{c}, \quad i = m, n. \quad (3)$$

There are  $N \cdot M$  recorded RF echoes in the STA method that are required for the synthesis of a single frame of a high resolution image. The synthesis is usually done off-line after the data acquisition cycle is finished. To achieve broadening of the transmit beam which is extremely important in cardiac imaging the concept of a virtual source is utilized in the STA. This modality is known in the literature as diverging wave imaging (DWI) (HASEGAWA, KANAI, 2011). Specifically, time delays in the transmit mode for each element are chosen in such a manner that the emitted wave can be considered as originating from a point source located at  $(x_\nu, z_\nu)$  (with respect to the sub-aperture center) behind the transmit sub-aperture as illustrated in Fig. 2. The virtual source can be shifted with respect to the center of the transmit sub-aperture. This results in an inclination of the wave-beam by an angle  $\Theta_i$ ,  $i = 0, \dots, I - 1$ . Therefore, there are  $M \cdot I$  emissions in each data acquisition cycle. The synthesized signal in diverging wave imaging with beam deflection can be

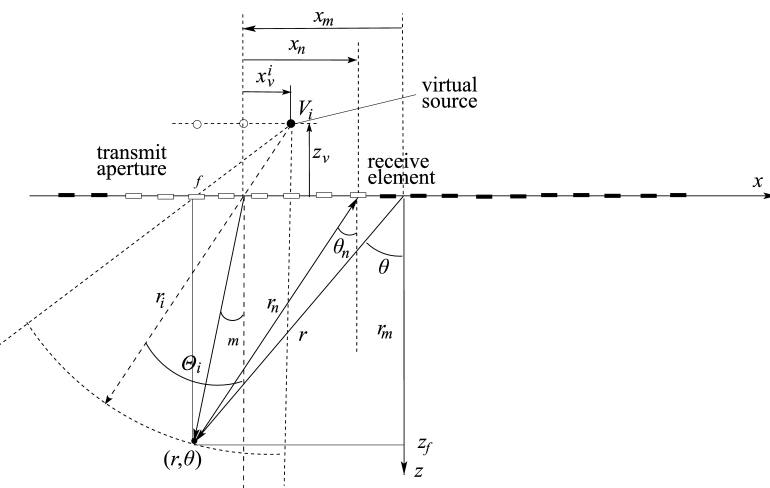


Fig. 2. Spatial diagram illustrating the geometry for the consideration of time delays applied to transducer elements for diverging wave transmission.

obtained by a coherent summation of all recorded RF echoes as follows:

$$A_{\text{DWI}} = \sum_{m=0}^{M-1} \sum_{i=0}^{I-1} \sum_{n=0}^{N_t-1} s_{m,n}^i (t - \tau_{m,n}^i), \quad (4)$$

where the round-trip delay  $\tau_{m,n}^i$  is comprised of two terms:

$$\tau_{m,n}^i = \tau_{m,n} + \tau_m^i. \quad (5)$$

The first term in Eq. (5) corresponds to the propagation delay of the scattered echo from the spatial point  $(r, \theta)$  to the  $n$ -th receive element transmitted by the  $m$ -th sub-aperture:

$$\tau_{m,n} = \frac{\sqrt{z_f^2 + (x_f - x_{m,n})^2}}{c}, \quad (6)$$

where

$$x_f = r \sin \theta, \quad z_f = r \cos \theta$$

are Cartesian coordinates of the focal point;  $x_{m,n}$  are coordinates of the  $n$ -th receive element in the  $m$ -th transmit sub-aperture (with respect to the sub-aperture center, see Fig. 2):

$$x_{m,n} = x_m - x_n = \left( -\frac{N-1}{2} + mN_{sh} - n \right) L. \quad (7)$$

In the above Eq. (7),  $L$  is the transducer pitch. The second term in Eq. (5) corresponds to the propagation delay of the emitted diverging wave to the spatial point  $(r, \theta)$ :

$$\tau_m^i = \frac{\sqrt{(z_f - z_\nu)^2 + (x_f - x_m + x_\nu^i)^2} - z_\nu}{c}, \quad (8)$$

for a given inclination angle  $\Theta = \tan^{-1} x_\nu^i / z_\nu$  (see Fig. 2). In Eq. (8),  $x_m$  is the transmit sub-aperture center:

$$x_m = \left( -\frac{N-1}{2} + mN_{sh} \right) L. \quad (9)$$

In Eq. (4), the first and second summation correspond to transmit beamforming, while the third one corresponds to receive beamforming. Each transmit sub-aperture comprised of  $N_t$  elements emits a diverging beam at specified angle of inclination  $\Theta_i$ . Backscattered echoes are independently recorded only by elements within the sub-aperture. Therefore,  $N_t \cdot M \cdot I$  recorded echoes are used for single frame synthesis in the diverging wave imaging approach described here.

### 3. Methods

The transmit/receive (TX/RX) data acquisition scheme implemented in the imaging method proposed in this paper covered the emission of diverging waves from a virtual source placed behind the transmit sub-aperture comprised of 32 transducers. The same sub-aperture was subsequently used in the receive mode. Next, the sub-aperture was translated by a distance of  $N_{sh} = 8$  transducer elements and the data acquisition was repeated. This required 5 TX/RX events to cover the full 64-element aperture and to reconstruct a single high resolution image.

Two different cases were considered separately. The first one corresponded to a single diverging wave emission in each sub-aperture location in the normal direction without beam steering. In the second case the beam steering in each transmit sub-aperture was implemented. Specifically, three diverging waves were emitted for each sub-aperture. The wave beam was steered in the directions of  $\{-20^\circ, 0, 20^\circ\}$ . This corresponded to 15 TX/RX events required to reconstruct a single high resolution image synthesized using the data from different virtual sources and sub-aperture locations, as discussed in the previous section.

To verify its performance, the method was tested using experimentally obtained synthetic aperture data of a custom-built phantom consisting of fine nylon wires ( $\varnothing 0.06$  mm), placed in 20 columns, each spaced 5 mm apart laterally. In each column there were 15 wires spaced 5 mm axially. Such an arrangement of point reflectors, covering the entire imaging region, was considered to be convenient for the visual assessment of imaging quality in the whole area. It enabled the estimation of spatial resolution at different depths, using corresponding lateral cross-sections of 2D images. The lateral resolution was quantified here by the full width at half maximum (FWHM). Additionally, an a Multi-Purpose Multi-Tissue Ultrasound Phantom, Model 040GSE (Computerized Imaging Reference Systems, Incorporated (CIRS), Norfolk, Virginia (Phantom, 2018)) was used in the experiments. The visualized region of the phantom consisted of a collection of cysts with diameters of 2, 4, and 8 mm, being representative of those encountered in clinical practice. The cysts were distributed at various depths which enabled the comparison of image contrast ( $C$ ) and contrast-to-noise ratio (CNR) obtained with different algorithms. Contrast and CNR were quantified using the following definitions:

$$C = \frac{|\mu_c - \mu_r|}{\mu_r} \quad (10)$$

and

$$\text{CNR} = \frac{|\mu_c - \mu_r|}{\sqrt{\sigma_c^2 + \sigma_r^2}}, \quad (11)$$

where  $\mu_c$  and  $\mu_r$  are mean intensities of cyst and reference regions; similarly,  $\sigma_c$  and  $\sigma_r$  are standard deviations for cyst and reference regions respectively. CNR and contrast  $C$  were evaluated at different depths for the cysts of diameter  $D = 8$  mm. The cyst region for each cyst was defined as the circle  $D_c$  of  $0.75D$  [mm] in diameter centered in the cyst origin for convenience. The corresponding reference region was defined as the circle  $D_r$  shifted laterally to the left by  $1.25D$  [mm] and having the same diameter  $0.8D$  [mm].

Moreover, the method proposed was verified using experimentally obtained data of the left ventricular phantom simulating transmural and non-transmural infarctions reported in (CYGAN *et al.*, 2017). This allowed investigating the ability to visualize moving objects. The model had the form of half of an ellipsoid with 15 mm wall thickness and 52 ml chamber volume when not deformed. It was deformed by applying pressure load to its inner surface. The wall deformation approximated that reported for the real heart. As reported in (CYGAN *et al.*, 2017) the deformation of the model acceptably correlated with clinical findings. The measurements were conducted at the Institute of Metrology and Biomedical Engineering, Warsaw University of Technology (Warsaw, Poland) in the same experimental setup as in reported work of CYGAN

*et al.* (2017) (see Fig. 2 of the cited paper). Specifically, it comprised a water tank with dedicated absorbers attenuating the reflected waves (Aptflex F28 and Aptflex F28P, Precision Acoustics, UK), tubing system, windkessel (to reduce/eliminate phantom vibrations), Vivitro Superpump with Vivitro Controller (Vivitro Labs Inc., Canada), with piston displacement curves corresponding to the volume change resulting from FEM simulations. The pump rhythm was set to 54 beats per minute. The data were collected with 1 kHz pulse repetition frequency. The frame rate of 100 fps was applied to accommodate the classical phased arrays imaging constraints (see discussion below).

The measurements presented in this paper were taken using the research system USPlatform (us4us Ltd., Poland) (LEWANDOWSKI *et al.*, 2012). The scanner was equipped with a standard 96 element phased-array transducer SP2430 (Esaote, Italy) excited by one cycle of the transducers center frequency equal to 2.3 MHz, 180 V (peak-to-peak) amplitude. To accommodate a 64-channel beamformer strategy only the 64 central elements of the transducer were excited. The radio frequency (RF) data collected on each of the 32 receive channels were digitized at a 12-bit resolution and a 50 MHz temporal sampling rate and transferred to a PC for further off-line processing in Matlab® in order to test the developed image reconstruction method.

The results obtained using the proposed diverging wave imaging (DWI) algorithm were compared with the images obtained using the classical beamforming phased array (PA) imaging. In this case the transmit beams were formed through applying appropriate delays to transmitting transducers, while the full working aperture (64 transducers) was used in each transmit and receive. 128 scan-lines were reconstructed to form a single high-resolution image in the PA method.

## 4. Results and discussion

### 4.1. Custom-design wire phantom imaging

Examples of 2D visualization of point reflectors are shown in Fig. 3 over a 30 dB dynamic range for two different TX/RX scheme, employing DWI and PA beamforming as discussed in the previous section. Specifically, in Fig. 3a the results obtained using DWI method for the virtual source located at  $z_v = -4$  mm and three wave beams steered in the directions  $\{-20^\circ, 0, 20^\circ\}$  is shown. In Fig. 3b results of DWI without beam steering is shown. And, finally in Fig. 3c the image reconstructed using PA beamforming method is shown. Each transmit beam was focused at the depth of 70 mm. The steering angles of the beams covered an imaged sector of  $90^\circ$ . In Fig. 4 the lateral cross-sections of the B-mode images shown in Fig. 3 at different depths are illustrated. They correspond to the point reflectors located in the central column of

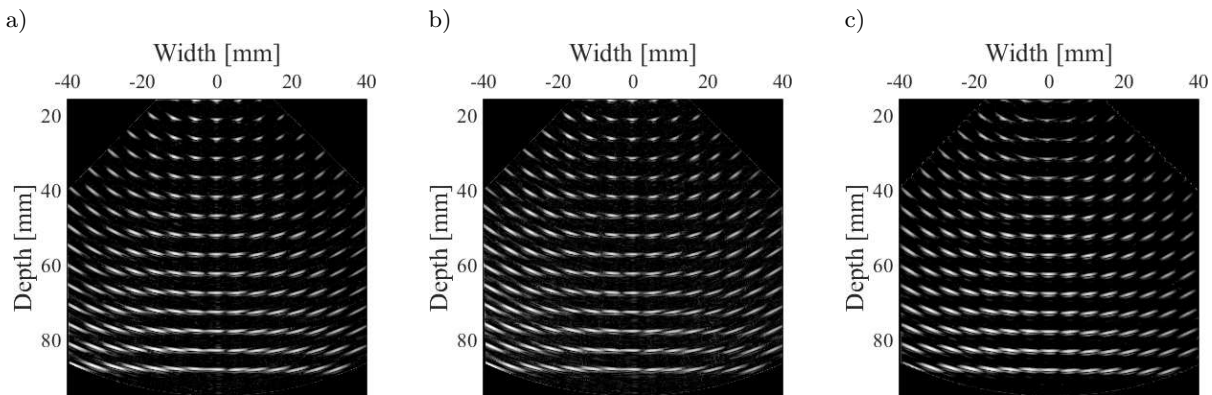


Fig. 3. Image reconstruction of the measurement data for a custom-built wire phantom for DWI method using 5 sub-apertures comprised of 32 transducers: a) three wave beams steered in the directions  $\{-20^\circ, 0, 20^\circ\}$  in each sub-aperture location, b) a single wave beam transmitted by each sub-aperture without beam steering, c) PA beamforming. All images are displayed over a 30 dB dynamic range.

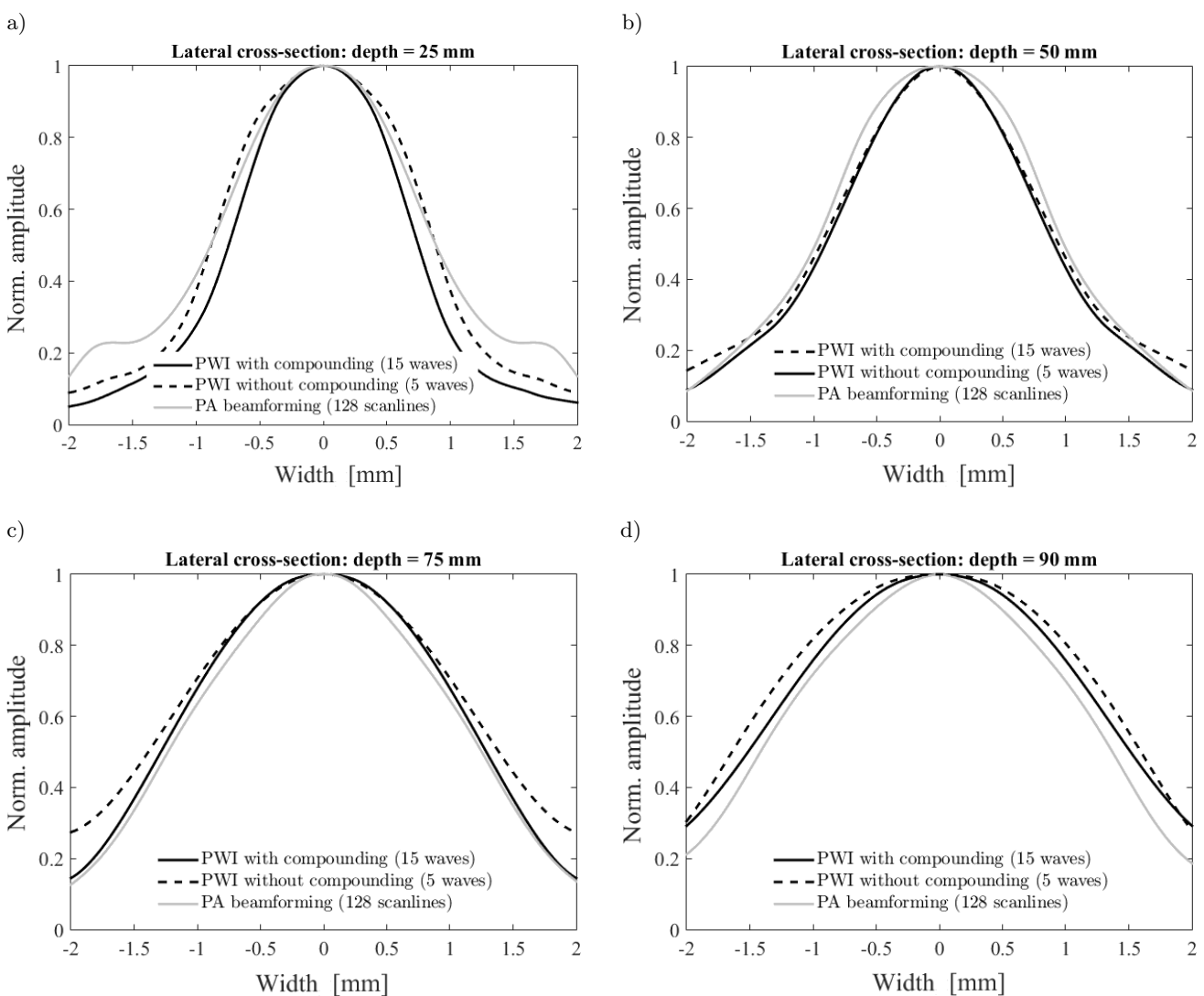


Fig. 4. Normalized lateral cross-sections of the B-mode images of point reflectors illustrated in Fig. 3 at different depths. Black solid line corresponds to DWI scheme with 5 sub-apertures comprised of 32 transducers and three wave beams steered in the directions  $\{-20^\circ, 0, 20^\circ\}$  in each sub-aperture location (15 waves transmitted per frame); black dashed line – DWI without beam steering (only 5 waves transmitted per frame); gray line – classical PA beamforming, 128 waves transmitted per frame, the steering angles of the beams covered an imaged sector of  $90^\circ$ .

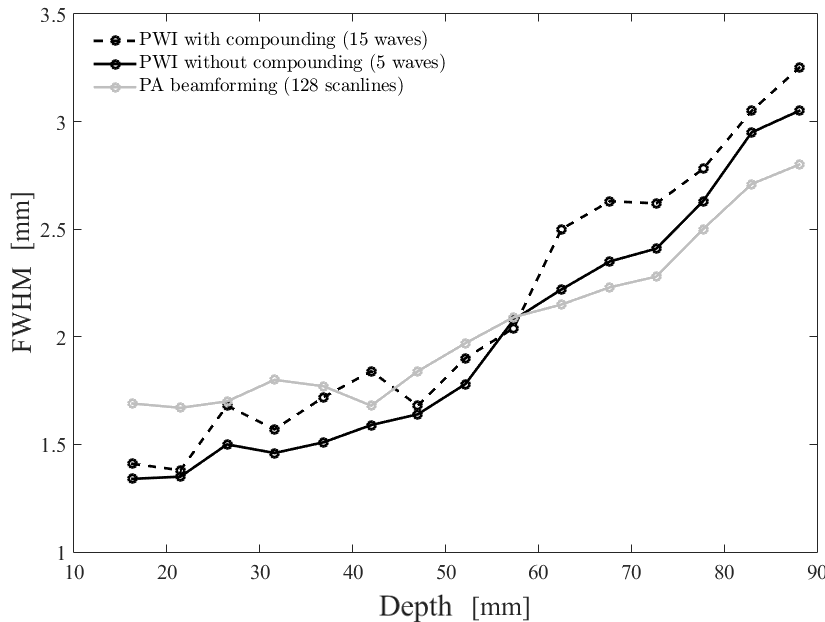


Fig. 5. FWHM versus depth assessed for the point reflectors located in center of the wire phantom in front of the probe midpoint. Black solid line – DWI scheme with 5 sub-apertures comprised of 32 transducers and three wave beams steered in the directions  $\{-20^\circ, 0, 20^\circ\}$  in each sub-aperture location (15 waves transmitted per frame); black dashed line – DWI without beam steering (only 5 waves transmitted per frame); gray line – classical PA beamforming, 128 waves transmitted per frame, the steering angles of the beams covered an imaged sector of  $90^\circ$ .

the wire phantom. The lateral cross-section shown in Fig. 4 give an indication of the resolution capabilities of different DWI schemes discussed above quantified here by the full width at half maximum (FWHM). Specifically, the results obtained using the DWI with 5 sub-apertures and 3 steering angle in each sub-aperture location (black solid line in Fig. 4) and a single wave emission without steering in each sub-aperture location (black dashed line) were compared to the classical PA beamforming. In Fig. 5 the resolution capabilities of the DWI method considered in Fig. 4 (quantified

here by the FWHM) versus depths are show. For comparison the results obtained using PA method are also presented. The lateral resolution was assessed for the same column of point reflectors located in center of wire phantom in front of the probe midpoint.

#### 4.2. Tissue mimicking phantom imaging

The contrast and CNR obtained for various TX/RX schemes were assessed in an experiment using a Multi-Purpose Multi-Tissue Ultrasound Phantom,

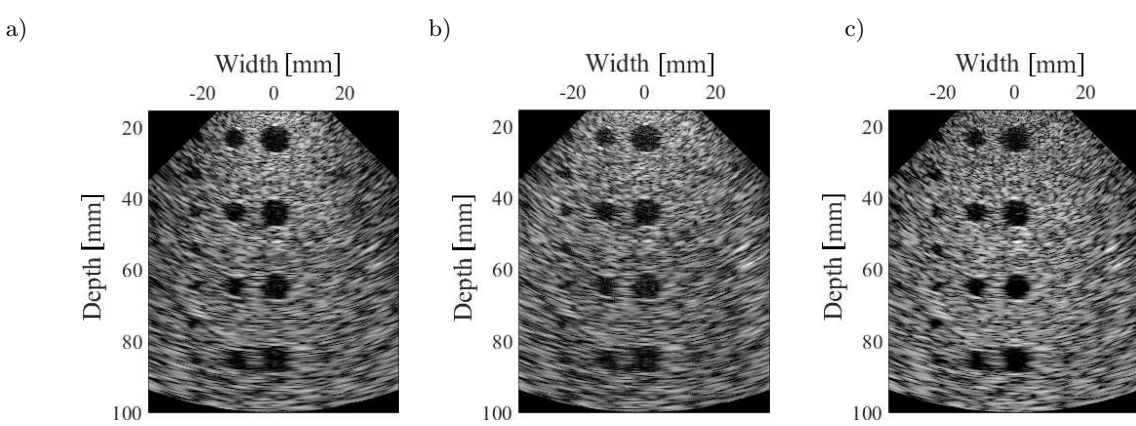


Fig. 6. Image reconstruction of experimental data obtained using Multi-Purpose Multi-Tissue Ultrasound Phantom, Model 040GSE (Computerized Imaging Reference Systems, Incorporated (CIRS), Norfolk, Virginia (Phantom, 2018)). a) DWI scheme with 5 sub-apertures comprised of 32 transducers and three wave beams steered in the directions  $\{-20^\circ, 0, 20^\circ\}$  in each sub-aperture location (15 waves transmitted per frame), b) DWI without beam steering (only 5 waves transmitted per frame), c) classical PA beamforming, 128 waves transmitted per frame, the steering angles of the beams covered an imaged sector of  $90^\circ$ .

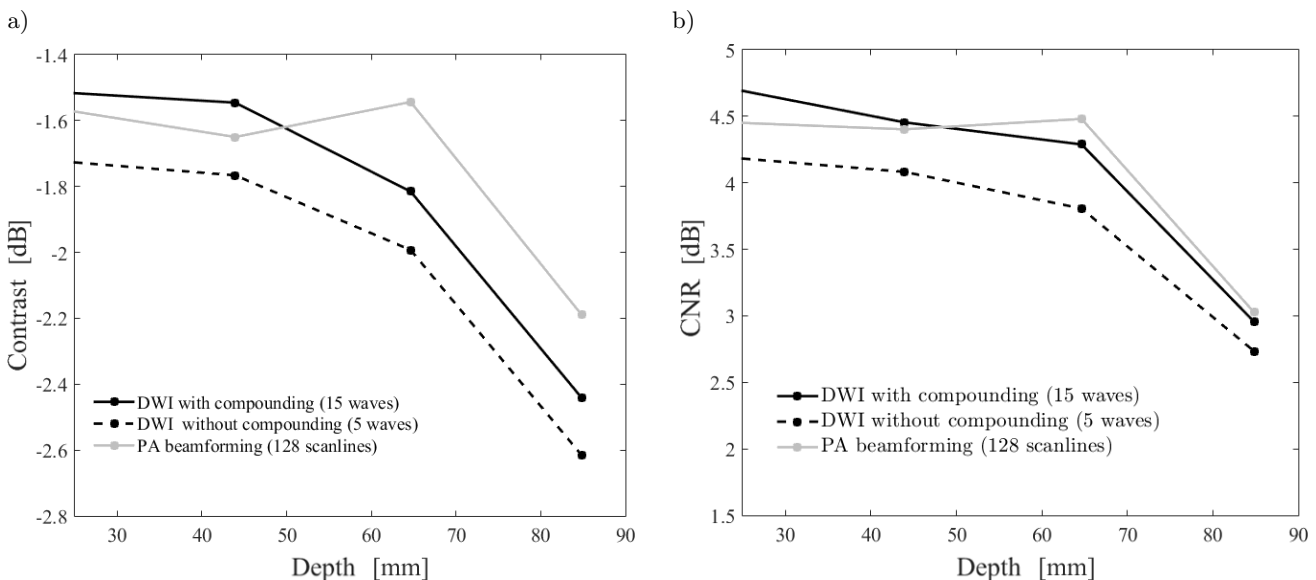


Fig. 7. Contrast (a) and CNR (b) evaluated for cysts at different depths for the images shown in Fig. 6. Black solid line – DWI scheme with 5 sub-apertures comprised of 32 transducers and three wave beams steered in the directions  $\{-20^\circ, 0, 20^\circ\}$  in each sub-aperture location (15 waves transmitted per frame); black dashed line – DWI without beam steering (only 5 waves transmitted per frames); gray line – classical PA beamforming, 128 waves transmitted per frame, the steering angles of the beams covered an imaged sector of  $90^\circ$ .

Model 040GSE (Computerized Imaging Reference Systems, Incorporated (CIRS), Norfolk, Virginia (Phantom, 2018)) data. Examples of 2D image reconstruction are shown in Fig. 6 over a 40 dB dynamic range for two strategies of the TX/RX scheme, which employ the DWI with the virtual source located at  $z_v = -4$  mm with compounding of three diverging waves steered in the directions  $\{-20^\circ, 0, 20^\circ\}$  in each sub-aperture location, Fig. 6a, and without beam steering, Fig. 6b, respectively. The sub-aperture comprised of 32 elemental transducers and sub-aperture translation distance of  $N_{sh} = 8$  elements between TX/RX events was assumed as in the previous subsection. For comparison, in Fig. 6c a 2D visualization of the tissue-mimicking phantom, obtained using classical PA imaging, is shown. 128 beams were used for image reconstruction. Each transmit beam was focused at the depth of 70 mm. The steering angles of the beams covered an imaged sector of  $90^\circ$ . In Fig. 7 the contrast and CNR evaluated using Eqs. (10) and (11), respectively, for cysts located at different depths are shown. The reference region has been chosen as discussed in the Sec. 3. For comparison, the results obtained using classical PA beamforming are shown.

#### 4.3. Dynamic phantom imaging

Figure 8 below compares experimentally obtained images of the left ventricular phantom simulating transmural and non-transmural infarctions reported in (CYGAN *et al.*, 2017) for the DWI method with beam-steering in the directions  $\{-20^\circ, 0, 20^\circ\}$  in each

sub-aperture, Fig. 8a through Fig. 8c, DWI with 5 sub-apertures comprised of 32 transducers without beam steering, Fig. 8d through Fig. 8f, and classical PA beamforming, Fig. 8g through Fig. 8i. The images in Fig. 8 are shown over a 40 dB dynamic range and correspond to different phases of the phantom work cycle, separated by 10 ms time intervals.

#### 4.4. Discussion of the results

The spatial resolution of the proposed method was validated using fine nylon wires. For depths not exceeding approximately 50 mm, the values of the FWHM in the proposed DWI method were slightly lower than the ones obtained using classical PA beamforming. Specifically, near the transducer face at the depth of approximately 30 mm the values of FWHM obtained by the DWI technique with wave beam steering (black solid line in Fig. 5) and without beam steering (black dashed line in Fig. 5) were approximately 0.81 and 0.87 times the corresponding FWHM value obtained using PA beamforming (gray line in Fig. 5), respectively. On the other hand, for larger depth better lateral resolution was obtained by PA method. Specifically, at the depth of approximately 90 mm the values of FWHM obtained by the DWI technique with wave beam steering and without beam steering were approximately 1.09 and 1.17 times the corresponding FWHM value obtained using PA beamforming, respectively.

The contrast and CNR, defined by Eqs. (10) and (11), were validated using a Multi-Purpose Multi-Tissue Ultrasound Phantom, Model 040GSE (Com-

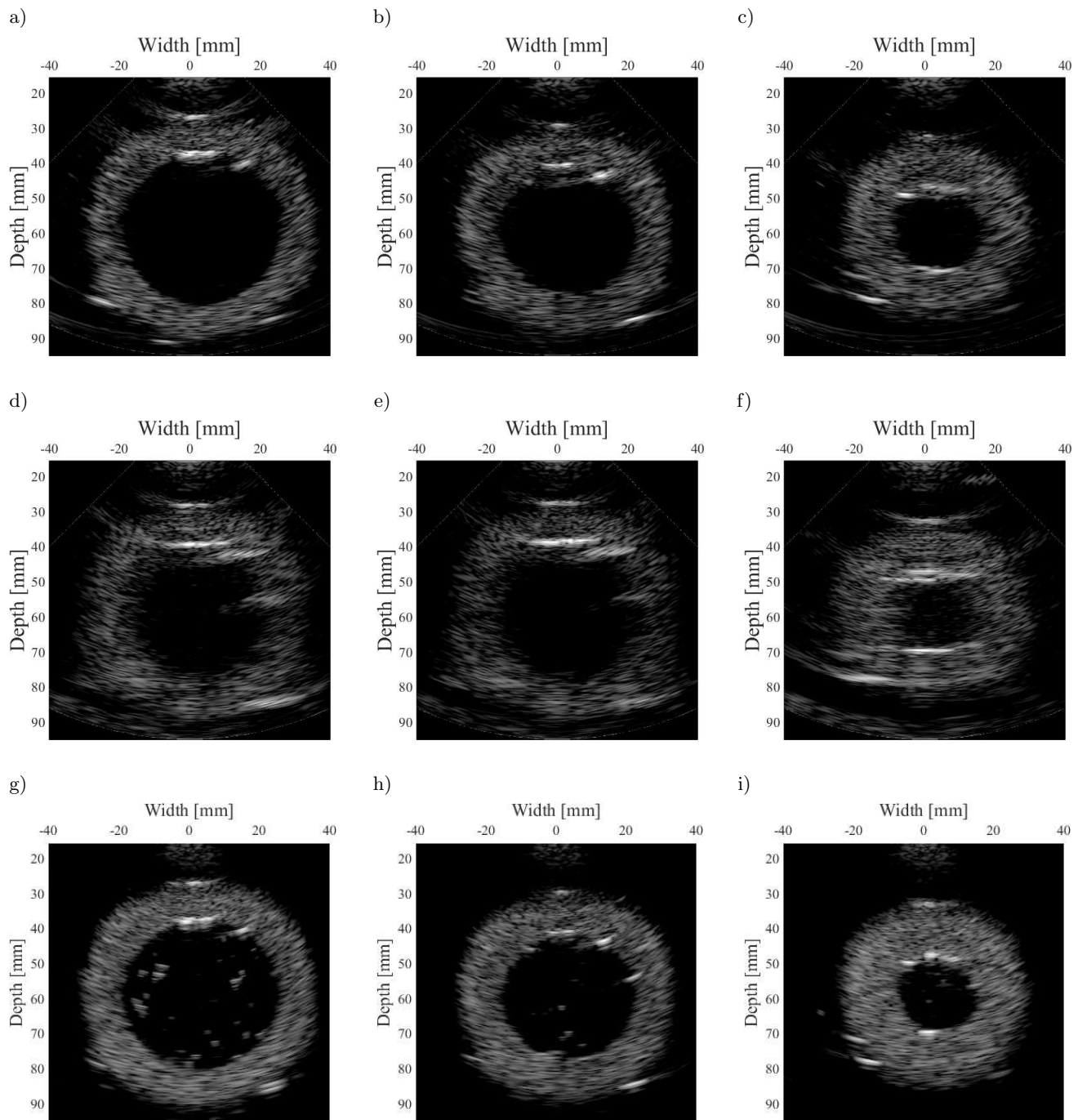


Fig. 8. Image reconstruction of experimental data obtained using a the left ventricular phantom: a) through c) DWI scheme with 5 sub-apertures comprised of 32 transducers and three wave beams steered in the directions  $\{-20^\circ, 0, 20^\circ\}$  in each sub-aperture location (15 waves transmitted per frame), d) through f) DWI without beam steering (only 5 waves transmitted per frame), g) through i) classical PA beamforming, 128 waves transmitted per frame, the steering angles of the beams covered an imaged sector of  $90^\circ$ . All images are displayed over a 40 dB dynamic range.

puterized Imaging Reference Systems, Incorporated (CIRS), Norfolk, Virginia (Phantom, 2018)). The contrast and CNR of B-mode images obtained by the proposed DWI method were slightly degraded for a visualization depth larger than 70 mm due to the increased side-lobe level in comparison to classical PA beamforming, as can be seen from Fig. 7. Specifically,

at the depth of approximately 80 mm the values of the contrast and CNR obtained by the DWI technique with wave beam steering (black solid line in Fig. 7) were approximately  $-2.44$  dB and  $2.95$  dB and without beam steering (black dashed line in Fig. 7) the corresponding values of the contrast and CNR were  $-2.62$  dB and  $2.73$  dB, respectively. The correspond-

ing values of the contrast and CNR obtained using PA beamforming (gray line in Fig. 7) were  $-2.19$  dB and  $3.03$  dB, respectively. At a lower depth not exceeding approximately  $50$  mm, the contrast and the CNR provided by the DWI with beam steering were slightly better in comparison with PA method. Thus, near the transducer face at the depth of approximately  $30$  mm the values of the contrast and CNR were  $-1.51$  dB and  $4.7$  dB for DWI with beam steering and  $-1.57$  dB and  $4.45$  dB for PA method, respectively.

Finally, the ability of the proposed imaging method to visualize a moving objects was tested using the left ventricular phantom measurement data. From Fig. 8a through Fig. 8f for images reconstructed using DWI method a slight degradation of the image quality can be observed (more pronounced moving artifacts) in comparison with the results obtained using PA beamforming, Fig. 8g through Fig. 8f. This, however, can be an admissible trade-off between image quality and reconstruction speed in a low-cost portable systems considered in this paper. Specifically, the images in Fig. 8d through Fig. 8f were obtained with only  $5$  TX/RX events ( $5$  sub-apertures comprised of  $32$  elemental transducers and no beam steering) whereas the ones obtained using the classical PA beamforming, Fig. 8g through Fig. 8i required  $128$  TX/RX events to reconstruct a single frame. Despite the slight degradation of the parameters mentioned above, the quality of B-mode images of the nylon wire phantom and the tissue mimicking phantom provided by the DWI method was comparable to the results obtained by PA technique. Moreover, a frame rate of approximately  $400$  Hz can be realized with a full lateral field of view of approximately  $90^\circ$  for the case of DWI with  $5$  sub-apertures comprised of  $32$  transducers and three wave beams steered in the directions  $\{-20^\circ, 0, 20^\circ\}$  in each sub-aperture location (which yields  $15$  TX/RX events per frame). For comparison, the corresponding value which can be realized by conventional sector scanning is  $50$  fps for  $120$  mm visualization and  $128$  scan-lines considered here ( $128$  TX/RX events per frame). It was shown, that using the DWI with only  $5$  sub-apertures (translated by a distance of  $8$  elements between transmissions) comprised of  $32$  elemental transducers and a single TX/RX event for each sub-aperture location, the frame rate of approximately  $1200$  fps can be obtained without sensible image quality degradation (see Fig. 3 through Fig. 8).

## 5. Conclusion

In this paper, we conducted a feasibility study of the ultra-fast imaging method for low-cost handheld cardiac scanner systems. The discussed method was based on STA DWI approach. A standard phased-array probe was connected the research system

USPlatform (us4us Ltd., Poland). The method proposed in this study used  $32$  elemental transducers both in transmit and receive modes which were connected to  $32$  electronic channels in the corresponding way to accommodate the low-cost system requirements. The STA technique was used to reconstruct the final image. To achieve frame rate increase from approximately  $50$  fps for the standard PA beamforming method, assuming a  $120$  mm visualization depth and  $128$  scan-lines reconstructed per frame, to approximately  $400$  fps in the proposed method, the  $32$ -element transmit sub-aperture was laterally translated by an optimal distance of  $8$  elements between subsequent pulse emissions (TASINKEVYCH *et al.*, 2012a). For each sub-aperture position a compounding of  $3$  beam-steered waves was used. In this case  $15$  TX/RX events were required to obtain the final B-mode images.

The lateral resolution was validated using fine nylon wires. To evaluate the contrast and CNR, the Multi-Purpose Multi-Tissue Ultrasound Phantom, Model 040GSE (Computerized Imaging Reference Systems, Incorporated (CIRS), Norfolk, Virginia (Phantom, 2018)) measurement data was used. It was shown that the developed DWI method with a reduced number of electronic channels allowed the lateral resolution and contrast/CNR comparable with classical PA beamforming to be obtained for a visualization depth not exceeding  $50$  mm. Moreover, it was shown that near the transducer face at the depth of approximately  $30$  mm the  $18\%$  increase of the lateral resolution quantified by the FWHM, as well as  $5.8\%$  and  $4\%$  increase of the CNR and contrast, respectively, was obtained in the case of the DWI technique in comparison with the classical PA beamforming. For larger visualization depths ( $70$ – $90$  mm), a slight degradation of the above parameters was observed. However, the quality (by visual assessment) of B-mode images of the nylon wire phantom, the tissue mimicking phantom provided by both methods was comparable. It was also shown that the frame rate can be further increased to approximately  $1200$  fps without sensible image quality degradation, provided no compounding and beam steering are applied in the DWI. In this case only  $5$  TX/RX events were required to obtain the final B-mode images. Summarizing, diverging wave phased-array imaging with a reduced number of channels can be a well suited technology for low-cost, energy efficient, handheld cardiac scanners.

## References

1. BAE M.H., JEONG M.K. (2000), *A study of synthetic-aperture imaging with virtual source elements in B-mode ultrasound imaging systems*, IEEE Transactions on Ultrasonics, Ferroelectrics, and Frequency Control, **47**, 6, 1510–1519.

2. CIKES M., TONG L., SUTHERLAND G.R., D'HOOGE J. (2014), *Ultrafast Cardiac Ultrasound Imaging: Technical Principles, Applications, and Clinical Benefits*, JACC: Cardiovascular Imaging, **7**, 8, 812–823.
3. CYGAN S., KUMOR M., ŹMIGRODZKI J., LEŚNIAK-PLEWIŃSKA B., KOWALSKI M., KALUŻYŃSKI K. (2017), *Left ventricular phantoms with inclusions simulating transmural and non-transmural infarctions – FEM and EchoPAC study*, Medical Imaging 2017: Ultrasonic Imaging and Tomography, 1013918–1.
4. HASEGAWA H., KANAI H. (2011), *High-frame-rate echocardiography using diverging transmit beams and parallel receive beamforming*, Journal of Medical Ultrasonics, **38**, 3, 129–140.
5. LEWANDOWSKI M., WALCZAK M., WITEK B., KULESZA P., SIELEWICZ K. (2012), *Modular & Scalable Ultrasound Platform with GPU Processing*, Proc. 2012 IEEE Ultrasonics Symp., pp. 2071–2074.
6. MOORE C. et al. (2015), *Live high-frame-rate echocardiography*, IEEE Transactions on Ultrasonics, Ferroelectrics, and Frequency Control, **62**, 10, 1779–1787.
7. PAPADACCI C., PERNOT M., COUADE M., FINK M., TANTER M. (2014), *High-contrast ultrafast imaging of the heart*, IEEE Transactions on Ultrasonics, Ferroelectrics, and Frequency Control, **61**, 2, 288–301.
8. Phantom (2018),  
<http://www.cirsinc.com/products/all/67/>.
9. SERAPHIM A., PASCHOU S.A., GRAPSA J., NIHOY-ANNOPOULOS P. (2016), *Pocket-Sized Echocardiography Devices: One Stop Shop Service?*, Journal of Cardiovascular Ultrasound, **24**, 1, 1–6.
10. SULZBACH-HOKE L.M., SCHANNE L.C. (1999), *Using a portable ultrasound bladder scanner in the cardiac care unit*, Critical Care Nurse, **6**, 19, 35–39.
11. TASINKEVYCH Y., KLIMONDA Z., LEWANDOWSKI M., NOWICKI A., LEWIN P.A. (2013), *Modified multi-element synthetic transmit aperture method for ultrasound imaging: A tissue phantom study*, Ultrasonics, **53**, 570–579.
12. TASINKEVYCH Y., TROTS I., NOWICKI A., LEWANDOWSKI M. (2012a), *Optimization of the Multi-element Synthetic Transmit Aperture Method for Medical Ultrasound Imaging Applications*, Archives of Acoustics, **37**, 1, 47–55.
13. TASINKEVYCH Y., TROTS I., NOWICKI A., LEWIN P.A. (2012b), *Modified synthetic transmit aperture algorithm for ultrasound imaging*, Ultrasonics, **52**, 2, 333–342.
14. TONG L., GAO H., CHOI H.F., D'HOOGE J. (2012), *Comparison of conventional parallel beamforming with plane wave and diverging wave imaging for cardiac applications: a simulation study*, IEEE Transactions on Ultrasonics, Ferroelectrics, and Frequency Control, **59**, 8, 1654–1663.